ELSEVIER

Journal of Power Sources 81–82 (1999) 328–334

JOURNAL OF POWER SOURCES

www.elsevier.com/locate/jpowsour

Lithium insertion/extraction in pyrolyzed phenolic resin

Zhaoxiang Wang [1], Xuejie Huang, Liquan Chen *

Laboratory for Solid State Ionics, Institute of Physics, Chinese Academy of Sciences, P.O. Box 603, Beijing 100080, China

Abstract

The mechanisms for the high capacity of lithium insertion in low-temperature pyrolytic carbons are not fully understood though several models have been proposed. None of the existing models considers the reversible crystalline structural changes within a graphene layer in the discharge–charge processes. In this report, low-temperature pyrolytic phenolic resin and lithium ion cells made of it are characterized by Raman spectroscopy, XRD and elemental analysis as well as discharge/charge measurements. The linear relation is confirmed between the specific capacity of the low-temperature pyrolytic carbon and its H/C atomic ratio after eliminating the influence of the crystallite size to the capacity. It is found that the evolution of the Raman spectrum of the pyrolytic carbon electrode upon discharge and charge is quite different from that of the other forms of carbonaceous electrodes. Based on the characteristic Raman spectra and the discharge–charge curves of the carbon electrode, a breaking-recovery model of the weak C · · · H bond is suggested for the lithium insertion/extraction processes in the low-temperature pyrolytic carbon electrodes.

Keywords: Lithium insertion/extraction; Pyrolized phenolic resin; Carbon electrodes

1. Introduction

Safety considerations lead to the replacement of pure lithium by heavier carbonaceous materials, with the general formula Li_xC_6 as the anode for lithium ion batteries. Development of high capacity carbons has been the goal of many research groups and has recently been reviewed by Dahn et al. [1–3]. Disordered carbons are promising candidates of anode material due to their much higher reversible capacity than the graphite-like carbon anodes in lithium ion batteries.

The specific capacity of a pyrolytic or disordered carbon depends, at least, on the H/C atomic ratio of the material and its crystallite size. A linear relationship between the specific capacity and the H/C atomic ratio of the material has been established. However, the H/C atomic ratio and the domain size of the material often vary simultaneously on pyrolyzing the precursor. Therefore, the established relationship is not so reliable before eliminating the interference of the domain size. We have shown previously that the domain size of the pyrolyzed polyfurfuryl alcohol decreases with prolonging pyrolytic time below some pyrolytic temperature [4], though usually the domain size increases with increasing pyrolytic time. This implies that there might be a critical temperature at which the domain size of the pyrolyzed polymer precursor does not change with heat-treatment time (HT). This is important because it allows us to separate the factors that affect the specific capacity of a pyrolytic carbon electrode. In this way a more reliable relationship between the H/C atomic ratio and the specific capacity can be found. This will help to understand the roles of the hydrogen content and the lithium insertion/extraction mechanism in pyrolytic carbon anodes.

Several models have been suggested to explain the excess capacity of disordered carbon anode over the theoretical value of 372 mA h/g of graphite anodes [1–3,5–9]. However, to our knowledge, none of these models considers the possible crystalline structural changes within a graphene layer of the pyrolytic carbon anodes in the discharge–charge processes and correlates them with the excess reversible capacity of these disordered carbon materials.

In this report, we will pyrolyze phenolic resin at 650°C for different heating times and study the crystalline structural changes of the carbon electrodes during discharge (lithium insertion) and charge (lithium extraction) processes by Fourier transform (FT) Raman spectroscopy, XRD, galvonostatic discharge/charge cycling as well as

* Corresponding author. Tel.: +86-10-6258-2046; Fax: +86-10-6256-2605; E-mail: lqchen@aphy02.iphy.ac.cn

[1] Present address: School of Chemistry, University of St. Andrews, St. Andrews, Fife KY16 9ST, Scotland, UK.

0378-7753/99/$ - see front matter
PII: S0378-7753(99)00262-1

elemental analysis. Our investigation indicates that the reversible breaking-recovery of the weak C · · · H bond in the material, especially that with substantial hydrogen content, may be an important factor that contributes to the excess capacity over that of the graphitic carbons.

2. Experimental

Phenolic resin was synthesized from phenol and formaldehyde at a molar ratio of 1:1.3. Solidified phenolic resin was pyrolyzed at 650°C for different HTs in an Ar atmosphere. The pyrolyzed phenolic resin block was polished with Al_2O_3 sandpaper to eliminate the surface species and then washed ultrasonically in methanol for 30 min before it was milled to fine powder. The Raman spectroscopic and X-ray diffraction (XRD) measurements of the as-prepared samples have been described before [10,11].

Two kinds of carbonaceous electrodes were prepared based on different investigation purposes. On preparing the electrode for the specific capacity measurements, pyrolytic carbon powder was mixed with carbon black and polyvinylidene fluoride (PVDF), the latter was dissolved in cyclopentanone beforehand. The doctor-blade method was used to get a homogeneous slurry film on the copper foil. The film was dried in a vacuum oven (120°C) for more than 12 h prior to use. The weight ratio of pyrolytic carbon to carbon black to PVDF in the electrode film was 85 to 10 to 5. With the carbon film as the cathode, metallic lithium foil as the anode, 1 M $LiPF_6$/(EC + DMC) (1:1 in volume) as the electrolyte and Celgard® 2400 as the separator, Li/C cells were assembled in an argon-filled glove-box. Such cells were discharged and recharged galvonostatically at 200 $\mu A/cm^2$ current density between 0.0 V and 2.0 V in an argon atmosphere.

As to the carbon electrodes for the electrochemical treatment and later for the Raman spectroscopic study, they were prepared without any additives so as to make the composition of the electrode as simple as possible. Other treatment processes (other aspects of the electrode preparation, cell assembly and discharge/charge atmosphere) of the cell were the same as that for the capacity measurement. The Li/C cells with such electrodes were discharged and/or charged at a current density from 20 to 100 $\mu A/cm^2$ in an argon atmosphere to the required equilibrium voltage (Li/Li^+). For the sample with a voltage of 0.0 V and those that needed to be charged later, the cells were short-circuited for a few days after being discharged to ca. 0.1 V so as to ensure an exact equilibrium voltage of 0.0 V. All the voltages shown in this paper were the final values after the circuit cutoff for 24 h at least. Later the cells were dissembled in the glove-box and the copper-foil supported carbon film was sandwiched and sealed between two pieces of optical glass (the thickness of the glass as the incident window was 85 μm), ready for the Raman measurement.

3. Results and discussion

3.1. Structural characterization of phenolic resin pyrolyzed at 650°C

The XRD measurements of phenolic resin before and after pyrolysis at 650°C show quite different patterns. However, the patterns of phenolic resin pyrolyzed for different HTs (0 to 50 h) are quite similar to each other. This means that the crystalline parameters of phenolic resin pyrolyzed for 0 to 50 h are roughly the same though no further analysis to the patterns was carried out due to the wide and mixed (10) diffraction peaks of the materials.

Figs. 1 and 2 show, respectively, the Raman spectra of the pyrolytic carbon excited with 488 and 1064 nm laser lines. The narrow band at ca. 1590 cm^{-1} (in Fig. 2) was attributed to the G-band (E_{2g2}, G for graphite) and the broad band at ca. 1310 cm^{-1} (in Fig. 2) is assigned to the D-band (A_{1g}, D for disorder). The positions of these two bands move to ca. 1600 cm^{-1} and 1350 cm^{-1}, respectively, when the excitation line is changed to 488 nm. This is due to the dispersion effect of the carbon materials and has been discussed in detail in our previous report [10]. Different excitation lines were used because the G-line shows a significant enhancement effect when the photon energy of the excitation is approaching the resonance energy for the $\pi-\pi^*$ transition. Therefore, some fine spectral differences may be observed (if there are any).

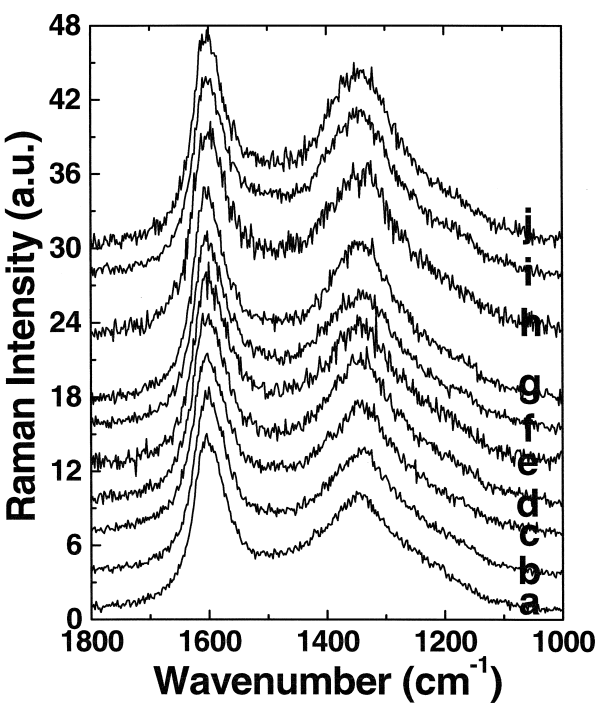

Fig. 1. Selected Raman spectra (excited with 488 nm) of pyrolyzed phenolic resin for different HTs at 650°C: (a) 0 h; (b) 2 h; (c) 4 h; (d) 6 h; (e) 8 h; (f) 10 h; (g) 20 h; (h) 30 h; (i) 40 h; and (j) 50 h.

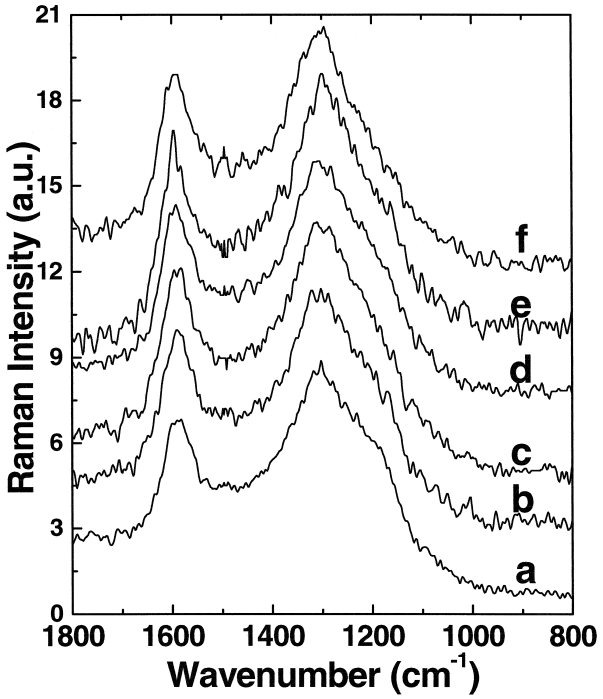

Fig. 2. Selected Raman spectra (excited with 1064 nm) of phenolic resin pyrolyzed at 650°C for different HTs: (a) 0 h; (b) 2 h; (c) 6 h; (d) 10 h; (e) 20 h; and (f) 50 h.

Here it is seen again that the Raman spectra of the phenolic resin pyrolyzed at 650°C for different HTs are quite similar to each other. Some spectral parameters are obtained to describe the crystalline features by fitting the Raman spectra. Figs. 3 and 4 show, respectively, the dependence of the integrated intensity ratios of I_G/I_D upon the pyrolysis time. Based on the Tuinstra–Koenig formula [12]

$$L_a(\text{nm}) = 4.4\, I_G/I_D \quad (1)$$

it is estimated that the domain size in the graphene layer (the L_a value) is ca. 3.0 nm and increased ca. 3% when the pyrolytic time is increased from 0 to 50 h.

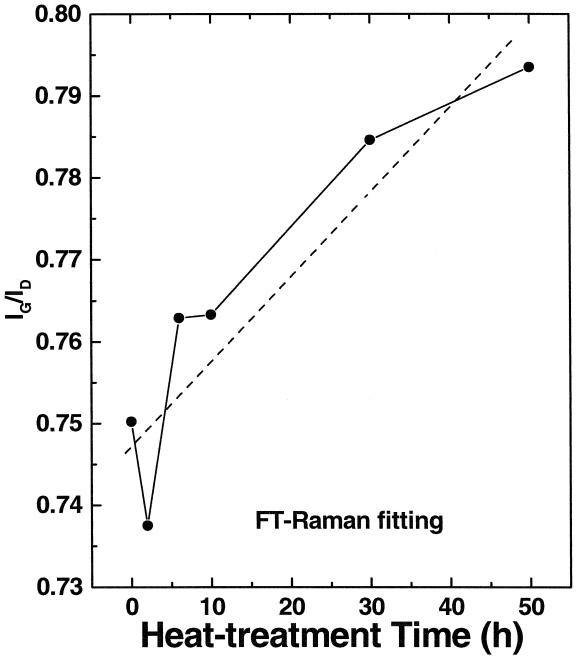

Fig. 4. HT dependence of the integrated intensity (1064 nm excitation) of the G-band to the D-band of phenolic resin pyrolyzed at 650°C.

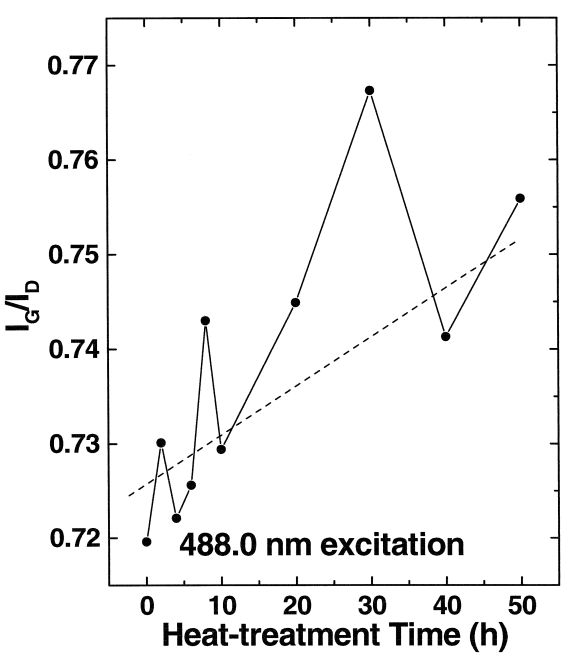

Fig. 3. HT dependence of the intensity ratio (488 nm excitation) of the G-band to the D-band of phenolic resin pyrolyzed at 650°C.

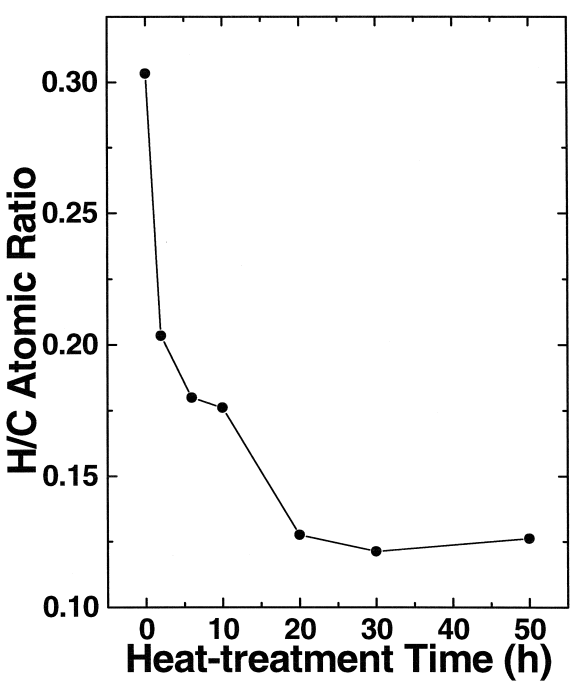

Fig. 5. Pyrolytic time dependence of the H/C atomic ratio in phenolic resin pyrolyzed at 650°C.

3.2. Correlation between H/C atomic ratio and specific capacity

Elemental analysis (Fig. 5) demonstrates that the H/C atomic ratio of the pyrolytic sample decreases from 0.32 to 0.12 during this process. Therefore, the change of the crystallite size is trivial in comparison with the drastic change of the H/C atomic ratio. This allows us to separate the two factors that affect the specific capacity of a pyrolytic carbon electrode, the crystallite size and the hydrogen content of the material.

A linear relationship is shown in Fig. 6 between the H/C atomic ratio and the specific capacity of the pyrolytic carbon electrodes. The specific capacity of the carbon electrode was determined from the average value of at least three Li/C cells. This linear relationship itself may seem to be nothing new because it just confirms the results of the previous reports [3]. However, the linear relationship shown here was obtained after eliminating the influence of the crystallite size on the specific capacity and is therefore more reasonable. As a result, it is helpful to the further understanding of the lithium insertion mechanism(s) in the pyrolytic carbon. Xiang et al. [9] believed that lithium is mainly doped at the edges of the graphene layers as well as between the graphene layers (forming GICs) and the excess capacity of the disordered carbon is proportional to the length of the graphene edge in a unit weight of the sample. Fig. 6 shows, however, that the crystallite size (L_a value) is not an essential factor that influences the excess capacity of the disordered carbon. Rather, the size factor blankets the H/C ratio factor because they often intermingle with each other and change simultaneously in the disordered carbons, especially upon organic precursors pyrolyzed at different temperatures. We suggest that it is the density of the lithium insertion sites along the edge of the graphene layer that determines the excess capacity rather than the edge length itself.

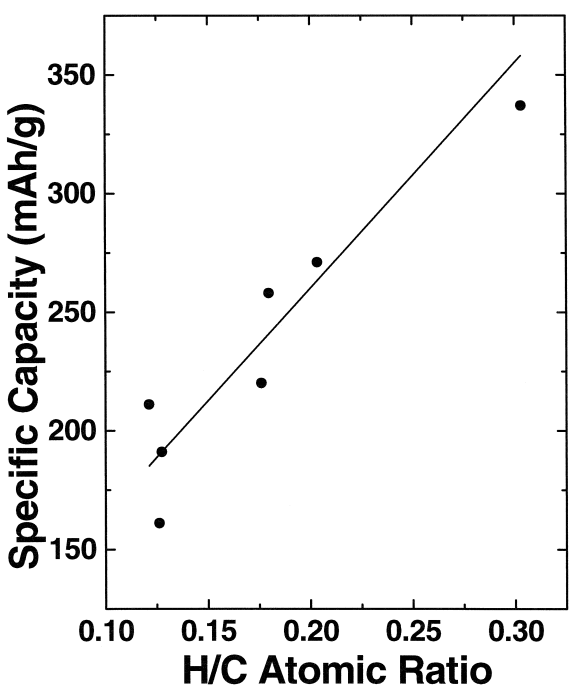

Fig. 6. The relationship between the specific capacity of the pyrolytic carbon anode and its H/C atomic ratio (the solid line is used to lead the eyes).

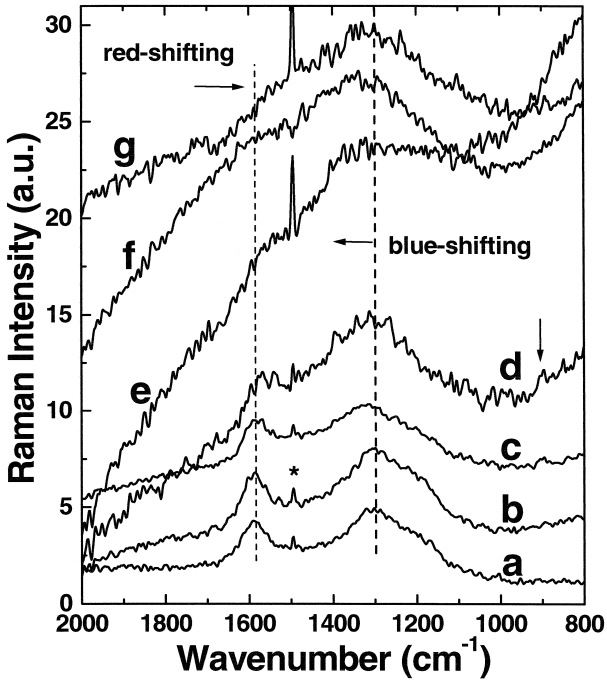

Fig. 7. Raman spectra of pyrolyzed phenolic resin discharged (lithium inserted) to different equilibrium potentials (Li/Li^+) in Li/carbon cells: (a) pristine pyrolyzed phenolic resin (before lithium insertion); (b) 0.83 V; (c) 0.51 V; (d) 0.17 V; (e) 0.10 V; (f) 0.04 V; and (g) 0.0 V (note: the weak bands at about 890 cm^{-1} with arrows overhead in this figure and in Fig. 9 are from the residue of the solvent; the sharp peaks with an asterisk overhead at about 1500 cm^{-1} are instrument errors).

3.3. Lithium insertion and extraction mechanism in pyrolytic carbon electrodes

In order to study the crystalline structural changes during the discharge–charge process and to understand insertion–extraction mechanism of lithium in pyrolytic carbon electrodes, Raman spectroscopic measurements were carried out on samples discharged and charged to different depths. Fig. 7 shows the Raman spectra of the pyrolytic carbon electrodes discharged to different equilibrium voltages. The spectral characteristics of Fig. 7 may be summarized as follows. Firstly, the relative intensity of the G-band to the D-band of the carbon decreases drastically with the drop of the discharge voltage. The G-band almost disappears at a voltage of about 0.10 V while the D-band remains until the end of discharge (0.0 V). Secondly, the width of the D-band increases slightly before the voltage reaches 0.10 V. Below that voltage the width of the D-band increases significantly until the end of discharge. Thirdly, the position of the G-band shifts towards the low

frequency side (red-shifting) with decreasing voltage while that of the D-band remains unchanged until the voltage of 0.10 V. Below 0.10 V, the position of the D-band shifts towards the high frequency (blue-shifting) in the spectrum. It seems that 0.10 V is a critical value in the discharge process.

Insertion of lithium between the graphene layers changes the electron density on the layer and weakens the intralayer C–C bonds. This explains the monotonous red-shifting of the G-band, characteristic of random lithium intercalation between graphene layers. However, none of the existing models can explain the abnormal variation of the intensity ratio I_G/I_D with discharging depth in the Raman spectra. Usually this ratio remains unchanged while lithium is inserted into natural graphite and HOPG electrodes. A simple analysis can exclude the possibilities that the remaining D-band is due to the decomposition of the binder PVDF or the formation of a passive film on the surface of the electrode. Therefore, the specific feature of the remaining D-band must have come from the crystalline structural changes of the Li-inserted disordered carbon itself. This is a phenomenon quite different from any of the previous observations in other carbons. It is characteristic of the pyrolytic carbon and may imply a lithium insertion mechanism different from that in other forms of carbons.

It has been well accepted that the relative intensity of the G-band to the D-band is closely related to the crystallite size of the sp^2-bonded carbon materials [13]. The crystallite size along the *a*-axis (L_a) is proportional to the ratio of I_G/I_D. Recently, Vidano et al. [14] suggested that only the G-mode should be used to determine the basal plane crystallite dimension L_a of the materials. Therefore, Fig. 7 indicates that in the meantime when the Raman scattering signal is reduced due to the increasing electrical conductivity of the electrode upon lithium insertion, the L_a value of the graphene layer also decreases when lithium is inserted into the carbon electrode. This could also be seen from the simultaneous increase of the width of the D-band upon lithium insertion.

Although there have not been any reports, to our knowledge, correlating the position shifting of the D-band with the structural changes of disordered carbons, an important fact is that the only band in the first-order Raman spectrum of severely disordered (amorphous) carbons is located at a higher frequency position than in less disordered carbons. For example, Yoshikawa et al. [15], and Ramsteiner and Wagner [16] reported, respectively, that the Raman bands of hydrogenated amorphous carbon (a-C:H) films are very broad (their full widths at half maximum, FWHMs, are larger than 100 cm^{-1}). Similar to the D-band in disordered carbons, this band in a-C:H films shows a more striking dispersion effect. Its position moves from 1600 to 1500 cm^{-1} when the excitation wavelength increases from an excitation photon energy of 3.54 eV (ca. 350 nm) to 2.18 eV (ca. 566 nm) [16]. Considering that the excitation wavelength in the present experiment is 1064 nm, it is understandable that the position of this band would red-shift further but is still at a frequency higher than the D-band of pyrolytic carbon, and overlaps with it, resulting in an observed blue-shift in the D-band. Therefore, the spectral changes of both the G- and D-bands in relative intensity, position and line width lead to the following conclusion: the weakening and disappearance of the G-mode, and the blue-shifting and the broadening of the D-band, imply that the graphene layer of the pyrolytic carbon electrode is damaged and becomes smaller in size. Finally, a structure similar to that of a-C:H (a-C:H-like) is formed upon lithium insertion.

Fig. 8 shows the Raman spectra of pyrolytic carbon charged to different equilibrium voltages. Clearly, this spectral evolution process is inverse to that of the discharged electrodes. Firstly, the relative intensity of the G-band increases while its width decreases with rising charge voltage till about 0.70 V. In the meantime, the position of the G-band shifts towards the high frequency with increasing voltage. Secondly, the line width and intensity (relative to that of the G-band) of the D-band decrease with rising voltage till 0.70 V. Thirdly, the position of the D-band remains unchanged until a voltage of about 0.90 V and then red-shifts obviously, opposite to the case below 0.10 V in Fig. 7. Above 0.70 V, the spectral features of both the G- and the D-bands become almost the same as their counterparts in pristine pyrolytic carbon (Fig. 8g). Based on the above discussion, it is reasonable to suggest that the fractured graphene layers

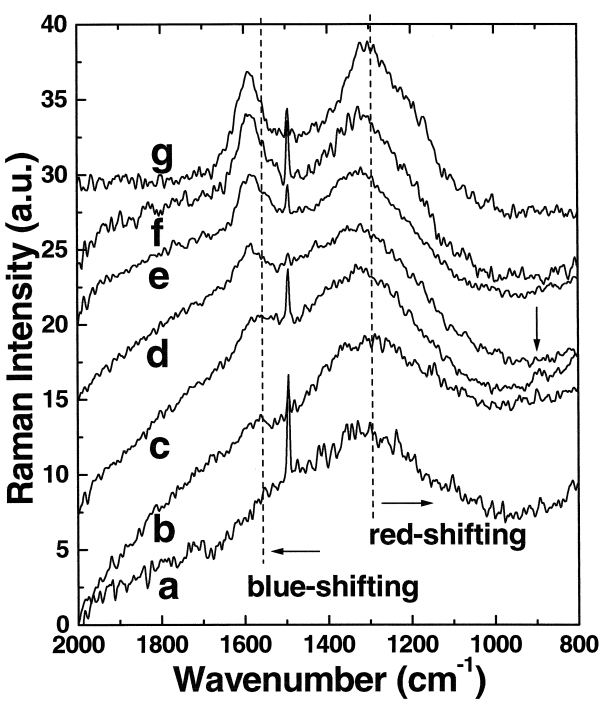

Fig. 8. Raman spectra of pyrolyzed phenolic resin charged (lithium extracted) to different equilibrium potentials (Li/Li^+) in Li/C cells: (a) 0.0 V; (b) 0.11 V; (c) 0.51 V; (d) 0.71 V; (e) 0.94 V; (f) 1.24 V; and (g) pristine pyrolyzed phenolic resin.

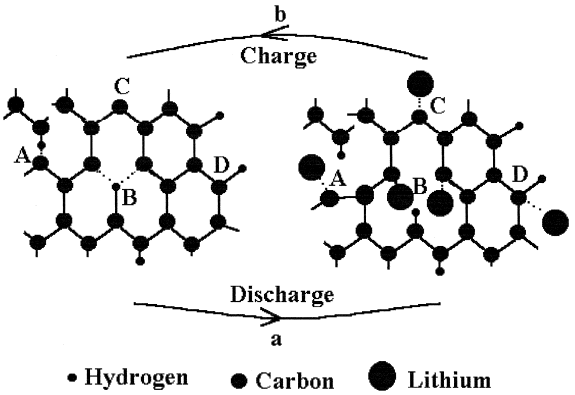

Scheme 1. A process of the crystalline structural changes of low-temperature pyrolyzed phenolic resin upon discharge (a) and charge (b): Site A, an edge point that connects two graphene layers by a weak C · · · H bond, which will be cleft on discharge; Site B, an inner nanopore where the hexagonal rings around it are connected by way of C · · · H bond; Site C, an edge point that transform the sp^2 bonding to sp^3 bonding on discharge and vice versa on charge; Site D, an edge carbon atom that has a dangling bond (note: (1) for brevity, the lithium ions inserted on and/or between the graphene layers are not schemed; (2) the two Li near Site B in the discharged electrode are not in the same graphene plane).

upon lithium insertion have, somehow, been connected, become larger and recovered to that of pristine pyrolytic carbon upon lithium extraction.

A brief review about the crystalline structural and electrochemical characteristics of pyrolytic carbon anodes will be helpful to understand the above suggestion. It is well known that there are a lot of imperfect hexagonal graphene rings in the low-temperature (below 1000°C) pyrolytic product. Therefore, it is understandable that there would be substantial amounts of carbon atoms with dangling bonds at the edge of the graphene layer and in the inner side of the micro- and nano-pores in the graphene layer. These dangling bonds may bind with the neighboring hydrogen atoms (the H/C atomic ratio is about 0.19 in the present pyrolytic carbon sample) to form weak C · · · H bonds (Scheme 1). Dahn et al. [1] studied the dependence of the electrochemical insertion of lithium in soft and hard carbons on the crystalline structures of the carbons and developed a structural model for disordered carbons. They believed that the insertion is a process from dilute to concentrated lithium ions between the graphene layers. That is, only the low-stage (stages 1 and 2) intercalation compounds can exist there. As a result, the Li–C interaction becomes stronger while the C–C bonding becomes weaker with increasing x in Li_xC_6. The case for the C · · · H bonds is similar to the C–C bond. Then the weak C · · · H bonds as well as the C–C bonds will be further weakened and the former are intended to be broken (Scheme 1a) when more lithium ions are inserted between the graphene layers. This process will lead to two effects. On one hand, the graphene intralayer size, L_a, becomes smaller and an a-C:H-like structure is formed. Therefore, the relative intensity of the G-band decreases to zero and only a broad D-band is observed in the Raman spectrum of fully lithium-inserted carbon electrode. On the other hand, breaking of the hydrogen bonds will create new sites for the inserted lithium ions to interact with the active carbon atom. The lithium ions may also bind quasi-reversibly at the hydrogen-terminated edges of graphene fragments in carbonaceous materials, causing a bonding change sp^2 to sp^3, as suggested by Dahn et al. [17–19].

In this way the positions that can accept lithium ions in a low-temperature pyrolytic carbon electrode are largely increased and the specific capacity of the carbonaceous anode is also raised, larger than that of natural graphite or HOPG where the number of the imperfect hexagonal rings is much smaller than in low-temperature pyrolytic carbons. On the other hand, when lithium ions are extracted from the anode (Scheme 1b), the lithium ions staying between the graphene layers are removed from the lattice. As a result, the electron density on the graphene layer decreases and the broken C · · · H bond is connected. So, an imperfect graphene layer grows in size and recovers to the structure of pristine pyrolytic carbon. The ratio of I_G/I_D also increases for the charged carbon electrode. In this process the extraction of the lithium ions coupled with the carbon atoms with dangling bond provide the excess Li-extraction capacity with respect to that of the natural graphite and HOPG. The G-band moves towards higher frequency due to the increasing C–C bonding when lithium is extracted from the graphene layer, and the D-band moves towards lower frequency when the content of a-C:H-like fragments becomes less. The above process is repeated when the next discharge/charge cycle begins.

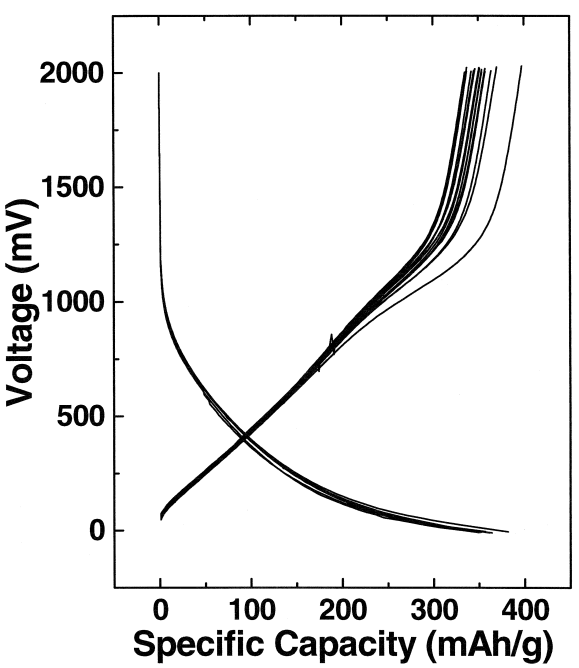

Fig. 9. Typical discharge–charge curves for the fifth to the twentieth cycles of a Li/C cell with phenolic resin pyrolyzed at 650°C for 2 h as the working electrode at a discharge/charge current density of 0.2 mA/cm^2.

Xiang et al. [9] have shown that carbons with the largest capacity for lithium are those with the largest fraction of single graphene sheets and with the smallest average micropore size. It is easy to understand that the larger the fraction of the graphene sheets and the smaller the average micropore size, the larger would be the number of edge sites and the more would be the dangling bonds and hydrogen-terminated sites. With more positions where the lithium is tended to be inserted to or extracted from, the reversible capacity of the disordered carbon electrode will be larger.

The above C · · · H bond breaking-recovery model not only explains the evolution of the Raman spectra of charged and discharged carbon electrodes, but also agrees quite well with the critical discharge–charge curves of the pyrolytic carbon electrodes (Fig. 9). It is seen that most of the lithium ions are inserted between 0.10 V and 0.0 V where there is no trace of the D-band in the Raman spectra (Fig. 7e, f and g). This implies that the excess reversible discharge capacity of pyrolytic carbon comes from the breaking of the C · · · H bond upon lithium insertion. In the charge profile is observed an obvious plateau at ca. 1.0 V which contributes the most to the total reversible charge capacities of low-temperature pyrolytic carbons [9]. This is the potential range that the ratio I_G/I_D changes dramatically in the Raman spectrum and the fractured graphenes combines to form larger domains. In the meantime, large amount of lithium is released from the loosely bound C · · · Li. So our model can well explain both the Raman spectral features and the critical discharge/charge profiles of the low-temperature pyrolytic carbons.

Our model suggests that the contribution of the structural changes in the scale of a graphene layer must be considered in understanding the excess reversible capacity of pyrolytic carbons over the graphitic carbons. Although there have been several models on the lithium insertion into carbonaceous materials, it seems that they all ignore the existence of the weak C · · · H bonds within the graphene layer and do not consider their influences on crystalline structures of the carbon anode upon discharging and charging. Therefore, it seems that the previous mechanisms, especially those concerning the lithium insertion in hard carbons where substantial amounts of hydrogen atoms exist and the single, bilayer and trilayer intercalation are the most important contribution to the capacity of the carbon anode, are far from perfect, if not incorrect.

4. Conclusions

In the above discussion, we have characterized the structural properties of phenolic resin pyrolyzed at 650°C for different times. A linear relationship is confirmed between the H/C atomic ratio in the pyrolytic carbon electrode and its specific capacity by excluding the possible perturbation of the contribution of the crystallite size to the specific capacity. Emphasis has been exerted on the analysis of the Raman spectral features of the Li/C cell electrodes discharged and charged to different equilibrium potentials. The Raman spectra indicate that breaking and recovery of the dangling bonds, as well as the previously reported quasi-reversible transformation of sp^2 to sp^3 hybridizations in near hydrogen-terminated sites upon lithium insertion, is responsible for the excess capacity of the disordered carbon anodes. On establishing a model for the lithium insertion–extraction in disordered carbon electrodes, especially those with a substantial content of hydrogen, the crystalline structural as well as the chemical structural changes are important factors to be considered.

References

[1] J.R. Dahn, A.K. Sleigh, H. Shi, J.N. Reimers, Q. Zhong, B.M. Way, Electrochim. Acta 38 (1993) 1179.
[2] J.R. Dahn, A.K. Sleigh, H. Shi, B.M. Way, W.J. Weydanz, J.N. Reimers, Q. Zhong, U. von Sacken, in: G. Pistoia (Ed.), Lithium Batteries, New Materials and New Perspectives, Elsevier, New York, 1993.
[3] T. Zheng, Y. Liu, E.W. Fuller, S. Tseng, U. von Sacken, J.R. Dahn, J. Electrochem. Soc. 142 (1995) 2581.
[4] G.-B. Li, Z.-H. Lu, B.-Y. Huang, Z.-X. Wang, H. Huang, R.-J. Xue, L.-Q. Chen, Solid State Ionics 89 (1996) 327.
[5] K. Sato, M. Noguchi, A. Demachi, N. Oki, M. Endo, Science 246 (1994) 556.
[6] A. Mabuchi, K. Tokumitsu, H. Fujimoto, T. Kasah, J. Electrochem. Soc. 142 (1995) 1041.
[7] R. Yazami, M. Deschamps, Proceedings of the 1994 MRS Fall Meeting.
[8] E. Peled, D. Golodnitsky, G. Ardel, C. Menachem, D. Bar Tow, V. Wshkenazy, Proceedings of the 1995 Spring MRS Meeting, San Francisco, 1995.
[9] H.-Q. Xiang, S.-B. Fang, Y.-Y. Jiang, J. Electrochem. Soc. 144 (1997) L187.
[10] Z.-X. Wang, X.-J. Huang, L.-Q. Chen, Carbon, 1998.
[11] Z.-X. Wang, Z.-H. Lu, R.-J. Xue, X.-J. Huang, L.-Q. Chen, J. Appl. Phys., 1998.
[12] F. Tuinstra, J.L. Koenig, J. Chem. Phys. 53 (1970) 1126.
[13] J.G. Naeini, B.M. Way, J.R. Dahn, J.C. Irvin, Phys. Rev. B 54 (1996) 144.
[14] R.P. Vidano, D.B. Fischbach, L.J. Willis, T.M. Loehr, Solid State Commun. 39 (1981) 341.
[15] M. Yoshikawa, G. Katagiri, H. Ishida, A. Ishitani, T. Akamatsu, J. Appl. Phys. 64 (1988) 6464.
[16] M. Ramsteiner, J. Wagner, Appl. Phys. Lett. 51 (1987) 1355.
[17] J.R. Dahn, T. Zheng, Y.-H. Liu, J.S. Xue, Science 270 (1995) 590.
[18] T. Zheng, J.X. Xue, J.R. Dahn, Chem. Mater. 8 (1996) 389.
[19] T. Zheng, W.R. McKinno, J.R. Dahn, J. Electrochem. Soc. 143 (1996) 2137.